International Journal of Automotive and Mechanical Engineering (IJAME)
ISSN: 2229-8649 (Print); ISSN: 2180-1606 (Online);
Volume 13, Issue 1 pp. 3262-3277, June 2016

DOI: http://dx.doi.org/10.15282/ijame.13.1.2016.12.0272

Characterization of the biaxial fatigue behaviour on medium carbon steel using the strain-life approach

S.A.N. Mohamed*, S. Abdullah, A. Arifin, A.K. Ariffin, and M.M. Padzi

Faculty of Engineering & Built Environment,
Universiti Kebangsaan Malaysia, 43600 Bangi, Selangor, Malaysia
Email: sityainy@siswa.ukm.edu.my
Phone: +60389118390; Fax: +60389259659

ABSTRACT

This study aims to investigate the fatigue behaviour and determine the fatigue life prediction under biaxial loading. Fatigue tests were performed according to ASTM 2207-02 and the values of tensile stresses are selected from the ultimate tensile strength which is 0.5 S_u, 0.6 S_u, 0.7 S_u, 0.8 S_u and 0.9 S_u, while the torsion angle representing the shear stresses acting was set at 15 degrees. The biaxial fatigue test was conducted using a combination of two types of stresses acting on the same frequency, namely 1 Hz, on smooth specimens made from medium carbon steel. The biaxial fatigue lives of the specimens are recorded when the specimen has completely fractured. The results indicate that the observed fatigue lives are in good agreement with the predicted lives by using the Coffin–Manson, Morrow, and Smith–Watson–Topper strain-based models. Mohr's circle approach was used to determine the maximum shear stress and principal normal stress. The maximum shear stress increased from 457 MPa to 486 MPa with the increment of principal normal stress from 612 MPa to 767 MPa. The principal stresses, maximum shear stresses, and energy dissipated were used to explain and describe the behaviour of biaxial fatigue. Both stresses are inversely proportional to the fatigue life. Meanwhile, the energy is linearly proportional to the stress applied, where the values increase in the range 500 kJ/m^3 to 605 kJ/m^3. Thus, the basic understanding of the material behaviour may be used in the processes of declaring component service lives and the fatigue life prediction of a particular automotive component. Therefore, the cost incurred can be reduced for the development process in material engineering.

Keywords: Cyclic hardening; maximum shear stress; multiaxial fatigue; principal normal stress; stress–strain hysteresis curve.

INTRODUCTION

Many engineering components and structures, such as axles, crankshafts, turbine discs, and blades, are exposed to complex and combined service loads that cause local multiaxial stress states on the critical material element. The accuracy of fatigue life estimation should be increased to understand the mechanism of damage accumulation subjected to service multiaxial loading [1]. Under service multiaxial loading, microscopic cracks can form and grow until macroscopic cracks are formed, thus causing damage to the component and structure. The behaviour of crack formation and propagation until the final fracture of materials under multiaxial stress states is different from that under the uniaxial stress state [2]. Therefore, multiaxial fatigue has become a popular topic in the past 20 years because of its great importance in mechanical design.

Some multiaxial fatigue models have been proposed for the prediction of multiaxial fatigue life [3-5]. A multiaxial fatigue model based on stress components was established by Shang et al. [6] using the linear relationship between the maximum normal stress and shear amplitude. The critical plane approach in multiaxial fatigue is based on the physical observation of crack initiation and growth in a particular plane assisted by the parameters in combinations involving damage to normal and shear stress on a plane [7, 8].

The automobile industries are always interested in innovations or research and development on the improvement of engine performance and operational service life to fulfill market expectations. Engine components are subjected to constant to varying loads, which also vary in direction and cause component failure. The connecting rod plays an important role in the operation of the crankshaft in the engine. This component is connected to the piston in the engine to transmit the thrust of the piston to the crankshaft, thus converting the reciprocating motion into rotary motion in the operation. Other parts, such as the pin-end, shank section, crank-end, and bolt, are attached to provide a good clamp. Therefore, this component is considered to be exposed to complicated loading and the main failure modes of connecting rods are fatigue fracture, excessive deformation, and wear [9]. Developing an appropriate design that suits a series of multiaxial workloads is complicated [10]. Hence, the failure attributed to broken connecting rods has led researchers to investigate this matter further. A study on the design of a connecting rod presented a resistant method of failure on connecting rod design that improved the fatigue life slightly [11]. It was found that the occurrence of fatigue phenomena is closely related to the appearance of cyclic stresses within the connecting rod body.

Damage parameters have been proposed to predict multiaxial fatigue failure and most of them are limited to certain load cases [12]. The multi-axis analysis approach can be divided into three categories based on the stress, strain and energy [8]. In considering the strain measurement, it is good to correlate the parameters with the fatigue life [13]. The strain-based approach can be considered as an approach which describes the overall behaviour of both the elastic and inelastic region where applicable, to detect the local plastic strain of stress concentration with the ability to change the input parameters such as the load history, geometry and attributes to predict the monotonic and cyclic fatigue life of components [5, 8, 14]. The strain–life approach considers the nominal elastic stresses and how they are related to the life. The elastic–plastic load stress and strain represents a more fundamental approach to determine the number of cycles required to initiate a small engineering crack [15].

Most of the existing multiaxial fatigue analyses were developed by using a stress-based approach to predict fatigue for high-cycle fatigue (HCF). The disadvantage of the stress-life analysis method is that more consideration is placed on the nominal elastic stresses than on the plasticity effect. Hence, the method provides poor accuracy for low-cycle fatigue (LCF). The strain-based life prediction method provides a detailed analysis involving plastic deformation at a localized region and can be used proactively for LCF life prediction in the initial design stage. Therefore, this inspired the authors to move forward with the present investigation on the biaxial fatigue life assessment of automotive components by using the strain-based approach. The main purpose of this study is to determine the fatigue behaviour of steel under biaxial constant amplitude loading (tension/torsion). An experiment was conducted on a solid mild steel rod to characterize the biaxial fatigue behaviour in a strain–life curve. The correlation between fracture was defined. Furthermore, the relationship between principal normal stress and

maximum shear stress on the activated plane shows proportional linear increments to the applied load. The energy dissipated during the failure is illustrated in the stress–strain hysteresis loop. The area under the loop became larger with increasing applied loads.

THEORETICAL BACKGROUND

The analysis and design of components by using stress-based fatigue life is a conservative approach for a situation wherein only elastic stresses and strains are present. However, most of the components with stress concentration typically result in local plastic deformation. Under this condition, the strain-based approach is adopted for an effective prediction of the fatigue life of a component. On the basis of the proposal by Niesłony and Böhm [16], the relation of the strain amplitude (ε_a) and fatigue life in reversals to failure ($2N_f$) can be expressed mathematically in the following form:

$$\varepsilon_a = \varepsilon_a^e + \varepsilon_a^p = \left(\frac{\sigma_f^{'}}{E}\right)\left(2N_f\right)^b + \varepsilon_f^{'}\left(2N_f\right)^c \tag{1}$$

Equation (1) is called the strain–life equation, where $\sigma_f^{'}$ is the fatigue strength coefficient, *b* is the fatigue strength exponent, ε'_f is the fatigue ductility coefficient, *c* is the fatigue ductility exponent, and *E* is the modulus of elasticity. This equation is the foundation for the strain-based approach to fatigue. This equation is also the summation of two separate curves for the elastic and plastic strain amplitudes. Niesłony and Böhm [16] proposed another relationship when the mean stress effect is taken into account:

$$\varepsilon_a = \varepsilon_a^e + \varepsilon_a^p = \left(\frac{\sigma_f^{'} - \sigma_m}{E}\right)\left(2N_f\right)^b + \varepsilon_f^{'}\left(2N_f\right)^c \tag{2}$$

when the elastic part of the strain–life curve is modified by the normal mean stress, σ_m. [17] proposed the following mean stress correction:

$$\sigma_{\max}\varepsilon_a E = \left(\sigma_f^{'}\right)2\left(2N_f\right)^{2b} + \sigma_f^{'}\varepsilon_f^{'}E\left(2N_f\right)^{b+c} \tag{3}$$

where $\sigma_{\max}$ is the maximum stress and ε_a is the strain amplitude.

The problem of stress under combined loading can be simplified by first determining the states of stress caused by the individual loadings. Hence, the axial stress is calculated as follows:

$$\sigma_a = \frac{P}{A} \tag{4}$$

where *P* represents the amplitude load and *A* refers to the original minimum cross-sectional specimen area. Meanwhile, the shear stress due to torque is calculated as follows:

$$\tau_{\max} = \frac{16T}{\pi D_{original}^{\ 3}} \tag{5}$$

where *T* represents torque and $D_{original}$ represents the original specimen test diameter.

The most used equivalent stress criteria for ductile steels in the LCF and medium-cycle fatigue areas are the von Mises ($\sigma_{a\ EQ\ vM}$) and Tresca ($\sigma_{a\ EQ\ T}$) criteria. Von Mises theory was proposed by Huber in 1904 and was further developed by von Mises in 1913 and Hencky in 1925 [18]. Von Mises theory denotes that failure by yielding occurs

when, at any point in the body, the distortion energy per unit volume in a state of combined stress becomes equal to that associated with yielding in a simple tension test. The Tresca criterion was proposed by Tresca (1814–1885) [6]. This criterion predicts that yielding will start when the maximum shearing stress in the material is equal to the maximum shear stress at yielding in a simple tension test. For combined tension and torsion in phase loading, these criteria are described by the following equation:

$$\tau_{\max} = \left(\sigma_a + m^2 \tau_a{}^2\right)^{1/2} \tag{6}$$

where σ_a, τ_a = normal stress, shear stress loading amplitude; $m^2 = 3$ for the von Mises criterion and $m^2 = 4$ for the Tresca criterion. The equivalent strain is defined as follows:

$$\varepsilon_{aEQ} = \left(\varepsilon_a{}^2 + \frac{\gamma_a{}^2}{3} \right)^{1/2} \tag{7}$$

The construction of Mohr's circle is one of the few graphical techniques still used in engineering and provides a simple and clear picture of an otherwise complicated analysis. This circle is usually referred to as Mohr's circle after the German civil engineer Otto Mohr (1835–1918). He developed the graphical technique for drawing the circle in 1882 [9]. Mohr diagrams can conveniently illustrate the relationship between the plane orientation and the values of normal/shear stress. The horizontal axis contains the possible values for the normal stresses, whereas the vertical axis contains the values for the shear stresses. The Mohr circle completely represents the state of stress at a point in terms of the normal and shear components. By substituting σ_{xx}, σ_{yy}, and τ_{xy} in the equation, the principal normal and maximum shear stresses can be calculated as follows:

$$\sigma_{1,2} = \frac{\left(\sigma_{xx} + \sigma_{yy}\right)}{2} \pm \left[\left(\frac{\sigma_{xx}}{2} \right)^2 + \tau_{xy}{}^2 \right]^{1/2} \tag{8}$$

$$\tau_{xy} = \left| \max \frac{\left(\sigma_1 - \sigma_2\right)}{2}, \frac{\left(\sigma_2 - \sigma_3\right)}{2}, \frac{\left(\sigma_3 - \sigma_1\right)}{2} \right| \tag{9}$$

In constructing Mohr's circle, the centre and radius of the circle are calculated as follows:

$$\sigma_{ave} = \frac{\left(\sigma_{xx} + \sigma_{yy}\right)}{2} \tag{10}$$

$$R = \left(\sigma_{ave}{}^2 + \tau_{xy}\right)^{1/2} \tag{11}$$

Fatigue life can be characterized by steady-state behaviour. The stress–strain relationship becomes stable after rapid hardening or softening in the initial cycles corresponding to the first several percentages of the total fatigue life. The cyclic stable stress–strain response is the hysteresis loop. The hysteresis loop, defined by the total strain range ($\Delta\varepsilon$) and the total stress range ($\Delta\sigma$), represents the elastic plus plastic work on a material undergoing loading and unloading. Masing's assumption states that the stress amplitude versus strain amplitude curve can be expressed by the cyclic stress–strain curve:

$$\varepsilon_a = \varepsilon_a^e + \varepsilon_a^p = \frac{\sigma_a}{E} + \left(\frac{\sigma_a}{K'} \right)^{1/n'} \tag{12}$$

where E = elastic modulus, K' = cyclic strength coefficient, and n' = cyclic strain hardening exponent. To determine the change in stress, the following Masing's model is used:

$$\Delta\varepsilon = \frac{\Delta\sigma}{E} + 2\left(\frac{\Delta\sigma}{K'}\right)^{1/n'} \tag{13}$$

MATERIAL AND METHODS

The characterization of the fatigue life was conducted on mild steel. This material is a common form of steel that provides material properties that are acceptable for many applications. Solid specimens with 6 mm diameter were designed to follow the specification in the ASTM E8-01 (Figure 1). The chemical composition results are shown in Table 1 [19]. Subsequently, the specimens underwent a tensile test according to the ASTM E466 through the use of a universal testing machine (Figure 2) with a 100 kN load cell capacity. The purpose of the test is to determine the monotonic properties of the material. Biaxial testing was performed by using the servo-hydraulic biaxial fatigue test machine with a 25 kN load cell capacity (Figure 3). Testing was conducted following the requirements in ASTM E2207-02 on estimating the fatigue lives of materials under combined axial–torsional loading with load-controlled conditions. The testing was performed by using a sinusoidal waveform at a constant cyclic frequency of 1 Hz [18]. A set of applied stresses for the biaxial cyclic test was chosen in the range of 0.5 S_u to 0.9 S_u. However, torsion was set at approximately 15° for the twist angle (clockwise–anticlockwise) for all tension loads.

Table 1. Chemical composition of mild steel.

Composition	Value (%)
Carbon, C	0.45
Manganese, Mn	0.4
Sulphur, S	0.015 max
Silicon, Si	0.12
Phosphorus, P	0.015 max

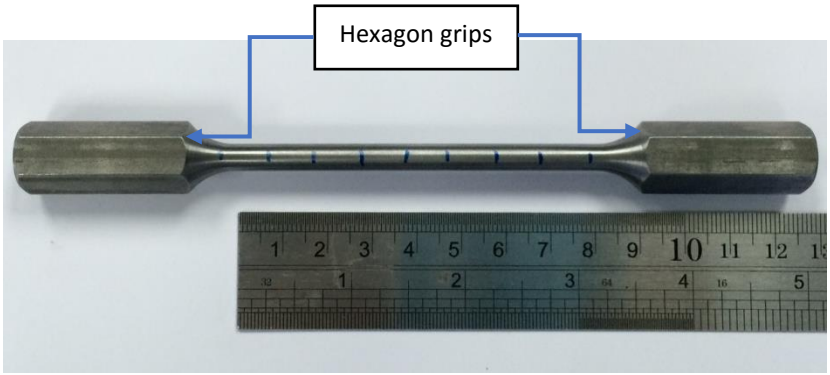

Figure 1. Specimen image after polishing process for both tensile and cyclic testing.

A finite element solution of the problem was obtained from a commercial finite element program to gain further insights into the effects of the loading modes. The input from the experiment was then fully used on the finite element program, such as the values of tension load (axial stress, σ) and torsion load (shear stress, τ). The results from the finite element analysis (FEA) were validated against the experimental results as illustrated in the correlation graph.

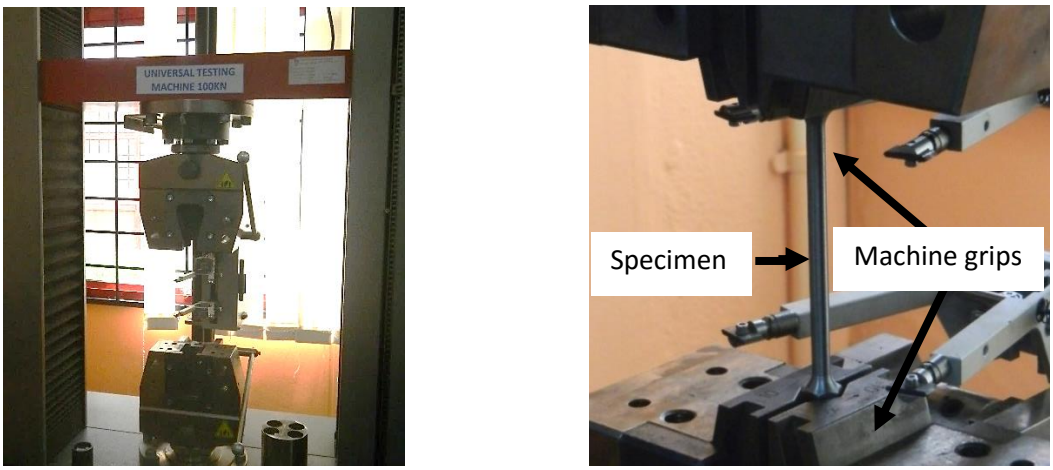

(a) (b)

Figure 2. Experiment setup for the tensile test: (a) Tensile machine used for the test, (b) solid specimen attached to the tensile machine grip.

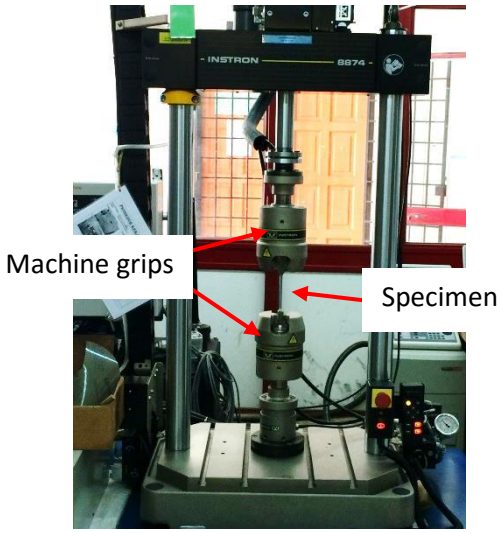

Figure 3. Servo-hydraulic biaxial fatigue machine.

RESULTS AND DISCUSSION

The monotonic properties of the mild steel, such as 623 MPa for ultimate tensile stress, 608 MPa for yield stress, and 220 GPa for Young's modulus, are obtained through the tensile test of the specimen and are tabulated in Table 2. It was found that the specimen exhibits ductile fracture, where the fracture surface shows moderate necking before the

break which is shown in Figure 4. The nature of ductile fracture is associated with a large amount of plastic deformation and occurs when the total stress (the sum of local stress, flow stress and hydrostatic stress) exceeds the interface bond strength [20]. The ultimate tensile strength is used as an indicator of a material limit stress at which the input parameters for the cyclic test. The Young's modulus is used to describe the elastic properties of material in the strain–life curve. The fatigue life of the experiment is shown in Table 3 for the five recorded values of equivalent stress from Eq. (6). The fatigue life of the mild steel is in the range of 10^0 to 10^2 cycles. Values for the experimental fatigue life are plotted in a log–log scale graph in Figure 5, which is calculated using the equivalent von Mises strain using Eq. (7), because this approach gives the same effect as a corresponding uniaxial strain state with the change to the value of the combined multiaxial strain [21].

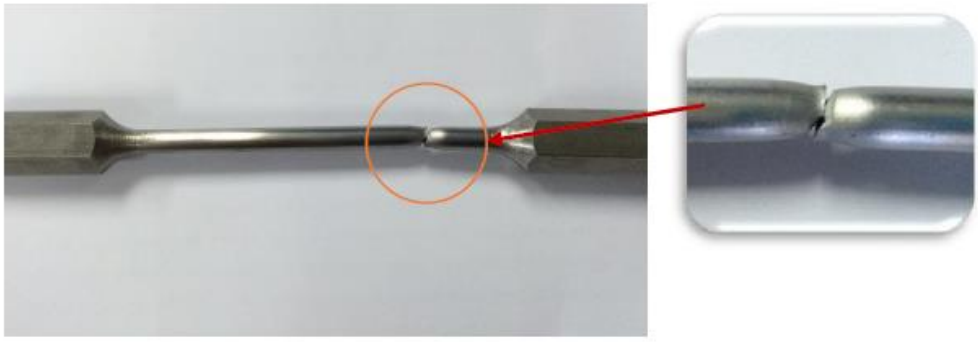

Figure 4. Necking fracture area of the specimen for tensile test.

Table 2. Experimentally determined monotonic properties of mild steel.

Properties	Value
Ultimate tensile stress, σ_u	623 MPa
Yield stress, σ_y	608 MPa
Young's modulus, E	220 GPa

Table 3. Fatigue life for constant biaxial loading.

Percentage of UTS value (%)	Equivalent stress (MPa)	Fatigue life (cycle)
50	805	106
60	821	104
70	843	46
80	859	44
90	888	36

Fatigue Life Assessment

Fatigue life results from the experiment were collected. The fatigue life from the simulations were calculated by using three different approaches, namely, Coffin–Manson (CM), Smith–Watson–Topper (SWT), and Morrow (M), which are expressed in Eqs. (1–3). The curve that represents the data in Figure 5 is called a strain–life curve

when the mean stress is zero. From the graph, the fatigue properties can be obtained, namely the fatigue ductility coefficient, ε_f' , fatigue ductility exponent, c, fatigue strength coefficient, σ_f', and the fatigue strength exponent, b. The fatigue ductility coefficient, ε_f', and fatigue ductility exponent, c are both material properties. Like the fatigue strength coefficient σ_f', also the fatigue ductility coefficient ε_f' is one-reversal intercept of the plastic curve and, therefore, it is equal to the true strain at fracture that represents the strain at which failure occurs after a half cycle under a monotonic load [22]. From Figure 5, the fatigue properties are determined as calculated in Table 4. The strain-based approach considers the plastic deformation that often occurs in localized regions where cracks nucleate and this comprehensive approach describes both the elastic and inelastic cyclic behaviour of a material [12].

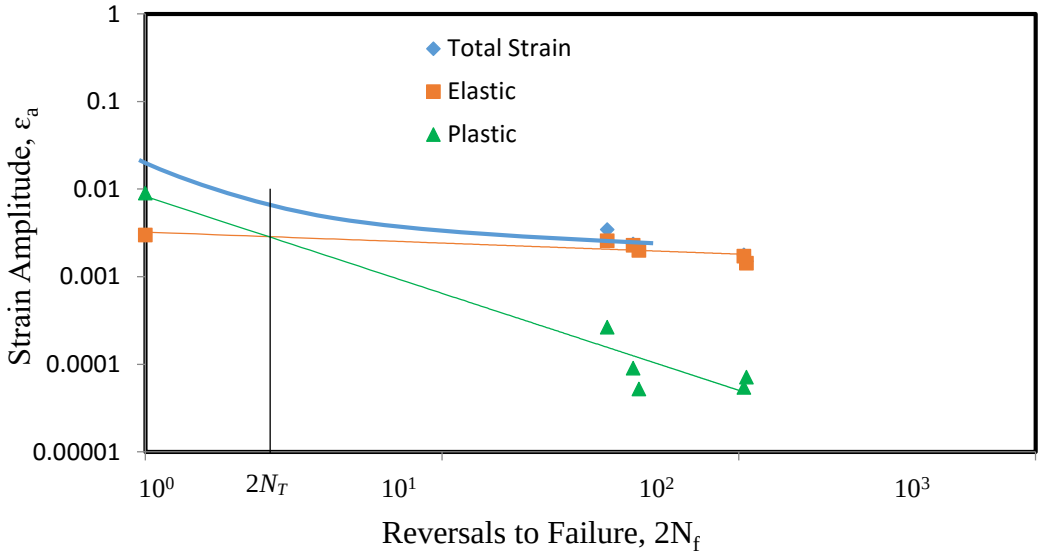

Figure 5. Strain–life curve for biaxial fatigue.

The values of the fatigue strength exponent and fatigue ductility exponent, which were obtained from the strain–life curve, are acceptable because both values are within the range of the metal's properties, where the value of the fatigue strength exponent b (as in the standard form) is between −0.04 and −0.15 and the fatigue ductility exponent c varies between −0.3 and −1.0 [23]. The exponent c is the slope of the plastic curve where the values significantly indicate the life of the material. Figure 5 shows that the intersection point of the linear elastic and plastic strain–life curve is referred to as the transition fatigue life ($2N_T$). The $2N_T$ is defined as the fatigue life when the magnitude of the plastic strain is equal to the elastic strain amplitude. The lower fatigue life region on the left of the transition fatigue life is considered the LCF, where the plastic strain occurs and is dominant. The high-fatigue life region on the right is the HCF, where the elastic strain is dominant.

Table 4. Fatigue properties for mild steel.

Properties	Value
Fatigue strength coefficient, σ'_f (MPa)	999
Fatigue ductility coefficient, ε'_f	0.03
Fatigue strength exponent, b	–0.10
Fatigue ductility exponent, c	–0.77

Fatigue life was then estimated by using the CM, SWT, and Morrow models. The equivalent strain data were plotted together in Figure 6. However, the consolidation shows that many of the points are plotted within the factor of 2:1, whereas a few points are located outside the correlation line. Thus, the experimental fatigue lives are acceptable and accurate [24] . The test results indicated that the fatigue life decreased in the experiment compared with the prediction life for the combined axial–torsion loading. The combined data plotted in the graph clearly shows that most of the points are within the error factor, while only a few points of 15% are located outside the line correlation, so this agrees with the von Mises criterion for steel [25]. The fatigue life for the three approaches is stated in Table 5. The experiment fatigue life is the closest to the Coffin–Manson prediction approach. This is because, in considering the situation in which the average stress value is zero, the Coffin–Manson approach provides accuracy in the calculation.

Table 5. Total fatigue life for experiments and simulations under biaxial stress of the mild steel.

Equivalent stress (MPa)	Fatigue life (cycle)			
	Experiment	Coffin–Manson	Morrow	SWT
805	106	78	47	70
821	104	41	27	38
843	46	24	16	22
859	44	15	11	14
888	36	5	4	5

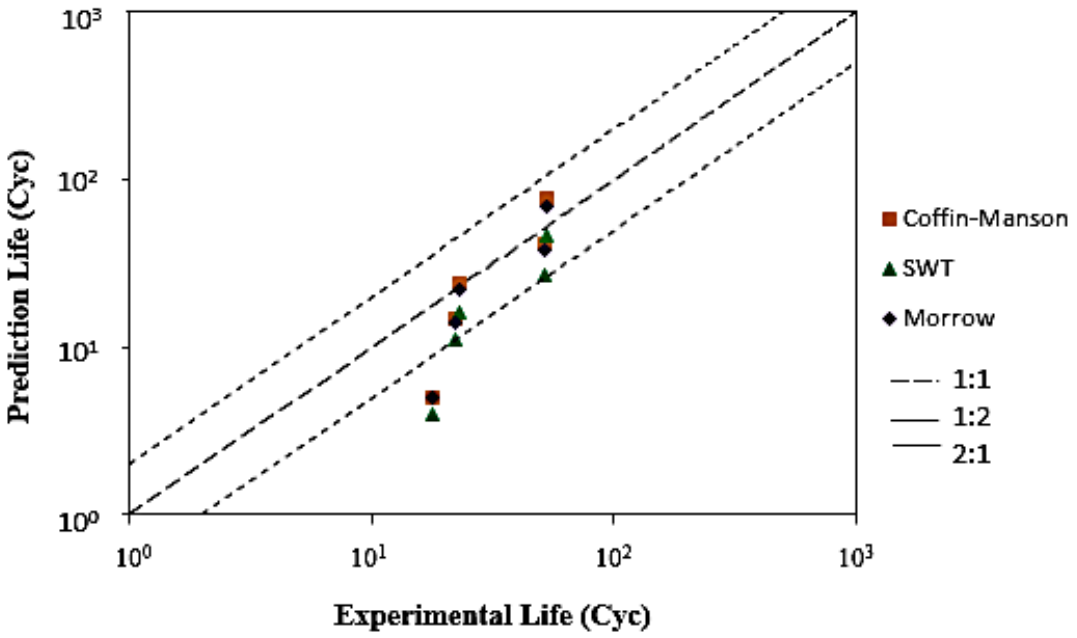

Figure 6. Relationship between predicted and experimental fatigue.

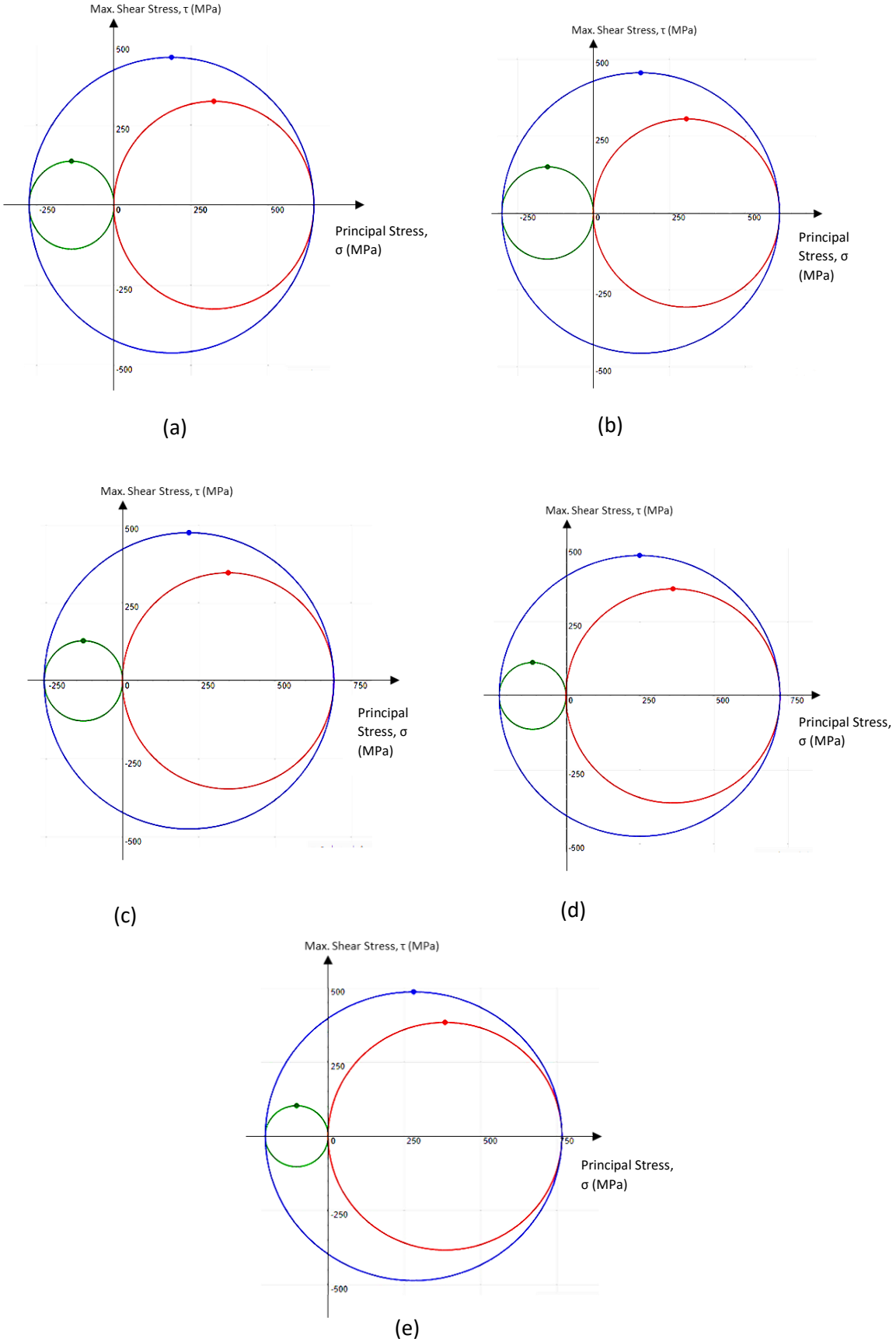

Figure 7. Mohr's circle for a 3D state of stress under biaxial loading from ultimate tensile stress (a) 0.5, (b) 0.6, (c) 0.7, (d) 0.8, and (e) 0.9 S_u.

Principal Normal Stress and Maximum Shear Stress on Mohr's Circle

The principal normal stresses and maximum shear stress on the inclined planes where the loads were acting can be calculated by using Mohr's circle. This graphical representation is extremely useful because it enables the visualisation of the relationship between normal and shear stresses acting on various inclined planes at a point in a stressed body. Two of the circles lie inside the largest circle, and each circle is tangent along the σ-axis to the other two, as shown in Figure 7. This result implies that the allowable normal stress refers to the principal normal stress and that the allowable shear stress refers to the absolute maximum shear stress. The allowable tensile normal stress refers to principal stress 1 (σ_1), where the load action is in tension. Furthermore, the allowable compressive normal stress refers to principal stress 3 (σ_3), which works in compression. In this case, the principal stress 2 (σ_2) is equal to zero because there is no load acting in that direction. Hence, the maximum shear stress refers to the highest point of the outer circle on the biggest Mohr's circle, the same value that is given by the radii of the circles. The trend expresses that increasing the load applied increases the values of σ_1 and τ_{max}. It shows the opposite trend for the value of σ_3. The values of the principal stresses increase and decrease in the range of about 5%–7%, as shown in Figure 8 and Table 6. The increments of the applied load tend to move the circle position to the right. The force acting on the plane (red circle) creates a uniform normal stress on the cross-sectional area of the specimen when tension load is applied to the tension plane, thus affecting the increase of the σ_1 value and τ_{max} and decreasing the value of σ_3 (green circle) (Figure 9). The activated plane indicates that not only is there normal stress but each stress is accompanied by shear stress.

Table 6. Normal stress and shear stress from the Mohr's circle analysis.

Applied load	Normal stress 1, σ_1 (MPa)	Normal stress 2, σ_2 (MPa)	Normal stress 3, σ_3 (MPa)	Maximum shear stress, τ_{maks} (MPa)
$0.5\sigma_{se}$	612	0	-300	456
$0.6\sigma_{se}$	648	0	-275	462
$0.7\sigma_{se}$	693	0	-257	474
$0.8\sigma_{se}$	724	0	-226	475
$0.9\sigma_{se}$	767	0	-206	486

The results shown in Mohr's circles clearly explain the different values and trends given on each of the stresses involved (Figure 8). The graph explains that σ_1 contributed significantly to fatigue failure. This result can be attributed to normal action of the principal normal stress on crack propagation, whereas the maximum shear stress was parallel to the crack plane. The observation indicates that cracks nucleate and grow on certain planes (critical plane) depending on the material and loading conditions (either maximum shear planes or maximum normal stress planes). Cracks as a result of the tensile stress categorized as formed in Mode I were affected by the maximum normal stress components. At this stage, the bonding strength of the structure is weak because of stress acting perpendicular to the plane. Therefore, the driving force leads to the nucleation of voids in the structure and then continues to crack growth, causing premature failure. Shear cracks form at the plane of maximum shear stress, and the process is failing in Mode II. In this case, the individual experiences the formation of

grain slippage when torsional load is acting parallel to the critical plane [26]. The graphic visualisation on Mohr's circle generates the idea of the relationship between the maximum shear stress and maximum normal stresses. The maximum normal stresses affect the value of the maximum shear stress on planes as they gradually increase. Therefore, this theoretical approach suggested that the parameters governing fatigue lives are related to the maximum shear strain or the combined effect of shear and stress normal to the plane of maximum shear strain. Thus, this approach evolved to deal analytically with multiaxial fatigue crack initiation and assumes that when the fluctuating state of strain at a critical location in an engineering component is the same as the strain in the uniaxial fatigue test specimen, a crack of similar proportions will develop in approximately the same number of fluctuations.

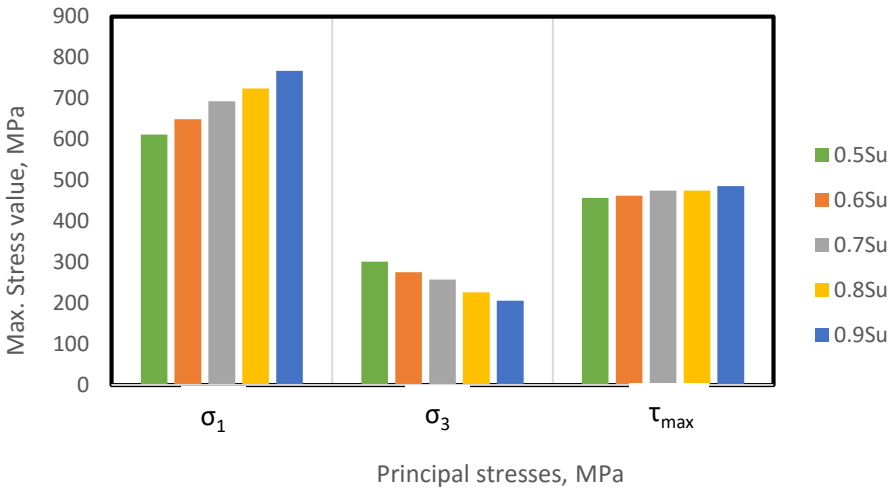

Figure 8. Principal normal stresses and principal shear stress trend value in Mohr's circle.

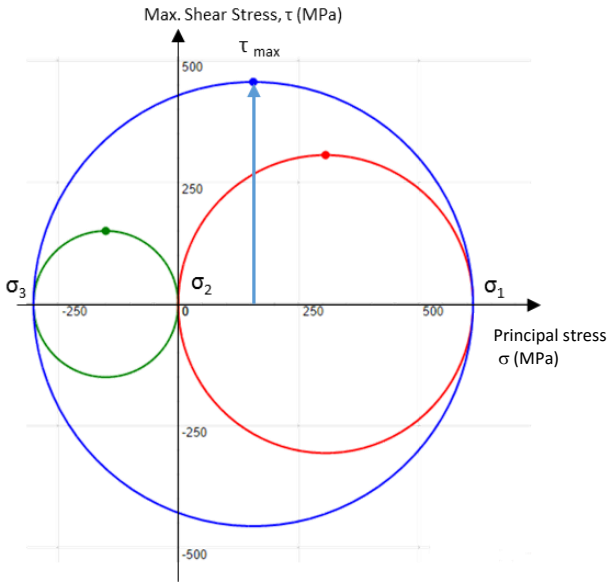

Figure 9. Mohr's circle representing the position of σ_1, σ_2, σ_3, and τ_{max}.

The behaviour of the biaxial fatigue is explained by the cyclic stress–strain relationship. Figure 10 demonstrates the shape of the hysteresis loop for mild steel under tension torsion loading. The hysteresis loop exhibits the elastic strain recovery as the large size of the area underneath loading and unloading curves. The area enclosing the hysteresis loop is equal to the amount of energy dissipated in the material upon the loading and unloading processes. Thus, the behaviour tends to show cyclic hardening with increasing $\Delta\sigma/\Delta\varepsilon$ [27]. When subjected to cyclic hardening, the process involved in fatigue deformation is the twinning–detwinning process, which plays a dominant role at the high strain amplitude. Dislocation slip dominates at the low strain amplitude. This result indicates that axial loading is the main cause of failure (Figure 11). Stress continually increases to drive the plastic deformation once the yield occurs.

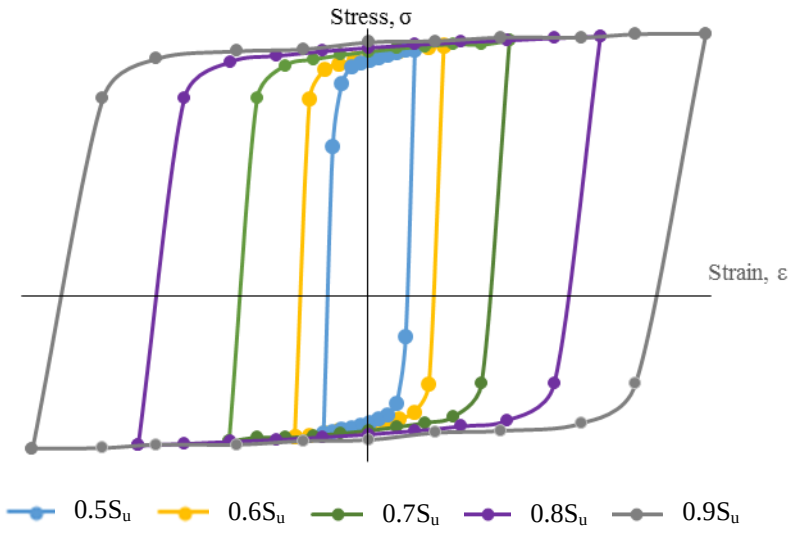

Figure 10. Hysteresis loop for biaxial fatigue.

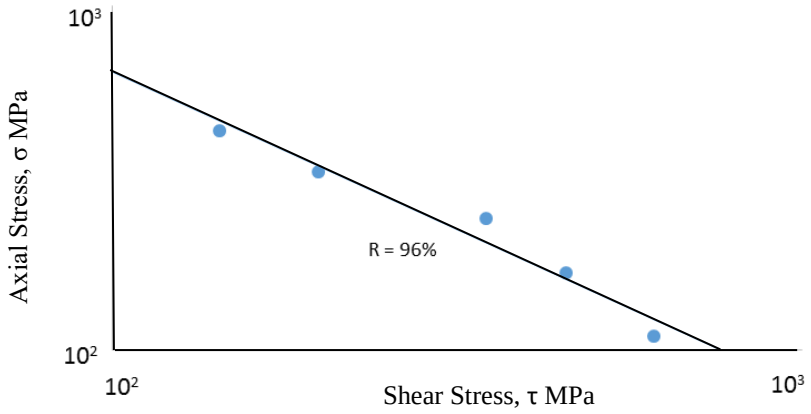

Figure 11. Correlation of shear stress and axial stress through material failure.

CONCLUSIONS

The strain–life curve for biaxial fatigue was plotted from the experiment results. The fatigue properties for mild steel were obtained from the curve. A good correlation was observed between the experimental fatigue life and predicted fatigue life. The behaviour showed that the biaxial fatigue life decreases with increasing stress. Individual loading in the biaxial fatigue provides a different impact on structure failure. The tension loads work perpendicular to the crack plane and contribute to the opening of cracks. On the contrary, shear stress acts in parellel yet has a small effect on crack growth. Finally, the domain of the structure failure depends on the tension loads that are applied when considering multiaxial fatigue. The normal stress obtained from the stress 0.5 S_u, 0.6 S_u, 0.7 S_u, 0.8 S_u and 0.9 S_u is 612 MPa, 648 MPa, 693 MPa, 724 MPa and 767 MPa, while the shear stress that is equivalent to the result of normal stress is 456 MPa, 462 MPa, 474 MPa, 475 MPa and 475 MPa. The increment of both stresses is in the range of 5%–7%. Biaxial fatigue behaviour is then discussed with the stress–strain diagram of relationships that form a cyclic hysteresis loop. The area within the hysteresis loop is equivalent to the total energy released when the process of loading and unloading occurs. The amount of energy produced by stress 0.5 S_u, 0.6 S_u, 0.7 S_u, 0.8 S_u and 0.9 S_u increases the number for each value of applied stress in the range 500 kJ/m^3 to 605 kJ/m^3, in which the lowest energy is produced by stress at 0.5 S_u and the highest energy is represented by the stress at 0.9 S_u. Through this investigation, the ideas may provide exposure and an overview on the characterization of biaxial fatigue loading**.** This result is significant as a basic overview for the initial stage of design to improve the fatigue life in normal operating loads for automotive components by knowing the maximum normal and shear stress that the components can sustain.

ACKNOWLEDGEMENTS

The authors would like to express their gratitude to Universiti Kebangsaan Malaysia through the fund of LRGS/2013/UPNM-UKM/DS/04 and the fund of FRGS/2/2014/TK01/UKM/02/3 for supporting this research project.

REFERENCES

[1] Kamal M, Rahman M. Fatigue life estimation models: a state of the art. International Journal of Automotive and Mechanical Engineering. 2014;9:1599.

[2] Itoh T, Sakane M, Ohsuga K. Multiaxial low cycle fatigue life under non-proportional loading. International Journal of Pressure Vessels and Piping. 2013;110:50-6.

[3] Liu J, Li J, Zhang Z-p. A Three-Parameter Model for Predicting Fatigue Life of Ductile Metals Under Constant Amplitude Multiaxial Loading. Journal of materials engineering and performance. 2013;22:1161-9.

[4] Abdul Majid MS, Daud R, Afendi M, Amin NAM, Cheng EM, Gibson AG, et al. Stress-Strain Response Modelling of Glass Fibre Reinforced Epoxy Composite Pipes under Multiaxial Loadings. Journal of Mechanical Engineering and Sciences. 2014;6:916-28.

[5] Kamal M, Rahman MM, Rahman AGA. Fatigue Life Evaluation of Suspension Knuckle using Multibody Simulation Technique. Journal of Mechanical Engineering and Sciences. 2012;3:291-300.

[6] Shang D-G, Sun G-Q, Deng J, Yan C-L. Multiaxial fatigue damage parameter and life prediction for medium-carbon steel based on the critical plane approach. International Journal of Fatigue. 2007;29:2200-7.

[7] Araújo J, Dantas A, Castro F, Mamiya E, Ferreira J. On the characterization of the critical plane with a simple and fast alternative measure of the shear stress amplitude in multiaxial fatigue. International Journal of Fatigue. 2011;33:1092-100.

[8] Golos KM, Debski DK, Debski MA. A stress-based fatigue criterion to assess high-cycle fatigue under in-phase multiaxial loading conditions. Theoretical and Applied Fracture Mechanics. 2014;73:3-8.

[9] Xu S-S, Nieto-Samaniego A, Alaniz-Álvarez S. 3D Mohr diagram to explain reactivation of pre-existing planes due to changes in applied stresses. International Symposium on In-Situ Rock Stress: International Society for Rock Mechanics; 2010.

[10] Kamal M, Rahman MM. Dual-Criteria Method for Determining Critical Plane Orientation for Multiaxial Fatigue Prediction Using a Genetic Algorithm. International Journal of Automotive and Mechanical Engineering. 2015;11:2571-81.

[11] Biancolini M, Brutti C, Pennestri E, Valentini P. Dynamic, mechanical efficiency, and fatigue analysis of the double Cardan homokinetic joint. International Journal of Vehicle Design. 2003;32:231-49.

[12] Ince A, Glinka G. A modification of Morrow and Smith–Watson–Topper mean stress correction models. Fatigue & Fracture of Engineering Materials & Structures. 2011;34:854-67.

[13] Kamal M, Rahman M, Rahman A. Fatigue life evaluation of suspension knuckle using multi body simulation technique. Journal of Mechanical Engineering and Sciences. 2012;3:291-300.

[14] Yunoh MFM, Abdullah S, Saad MHM, Nopiah ZM, Nuawi MZ. Fatigue Feature Extraction Analysis Based on a K-Means Clustering Approach. Journal of Mechanical Engineering and Sciences. 2015;8:1275-82.

[15] Rahman M, Noor M, Bakar R, Maleque M, Ariffin A. Finite element based fatigue life prediction of cylinder head for two-stroke linear engine using stress-life approach. Journal of Applied Sciences. 2008;8:3316-27.

[16] Niesłony A, Böhm M. Mean stress effect correction using constant stress ratio S–N curves. International journal of fatigue. 2013;52:49-56.

[17] Kwofie S, Chandler H. Low cycle fatigue under tensile mean stresses where cyclic life extension occurs. International Journal of Fatigue. 2001;23:341-5.

[18] Lowisch G, Bomas H and Mayr P.Fatigue crack initiation and propagation in ductile steels under multiaxial loading. Multiaxial and Fatigue Design, ESIS 21, Mechanical Engineering Publication, London, 1996; 243-59.

[19] Zarroug N, Padmanabhan R, MacDonald B, Young P, Hashmi M. Mild steel (En8) rod tests under combined tension–torsion loading. Journal of Materials Processing Technology. 2003;143:807-13.

[20] Pradhan P, Robi P, Roy SK. Micro void coalescence of ductile fracture in mild steel during tensile straining. Frattura ed Integrità Strutturale. 2012.

[21] Ion D, Lorand K, Mircea D, Karolv M. The equivalent stress concept in multiaxial fatigue. Journal of Engineering Studies and Research. 2011;17:53-62.

[22] Milella PP. Fatigue and corrosion in metals: Springer Science & Business Media; 2012.

[23] Castillo E, Fernández-Canteli A, Pinto H, López-Aenlle M. A general regression model for statistical analysis of strain–life fatigue data. Materials Letters. 2008;62:3639-42.
[24] Kim K, Chen X, Han C, Lee H. Estimation methods for fatigue properties of steels under axial and torsional loading. International Journal of Fatigue. 2002;24:783-93.
[25] Mohammad M, Abdullah S, Jamaludin N, Innayatullah O. Predicting the fatigue life of the SAE 1045 steel using an empirical Weibull-based model associated to acoustic emission parameters. Materials & Design. 2014;54:1039-48.
[26] Stephens RI, Fatemi A, Stephens RR, Fuchs HO. Metal fatigue in engineering: John Wiley & Sons; 2000.
[27] Landgraf R, Morrow J, Endo T. Determination of the cyclic stress-strain curve. Journal of Malterials. 1969;4:176-88.